Global NEST Journal, Vol 26, No 9, 06570

Optimization of the Freeze Crystallization Process for Recovering of Copper (II) Sulphate from Electroplating Wastewater Using Response Surface Methodology (RSM)

Yu Zhang[1,2], Zhihao Li[1,2], Cheng Gong[1,2], Xinxin Lv and Defeng Kong[1,2], Xing Chen[1,2]*
[1]School of Resources and Environmental Engineering, Hefei University of Technology, Hefei 230009, China
[2]Institute of Industry and Equipment Technology, Hefei University of Technology, Hefei 230009, China
Received: 31/07/2024, Accepted: 26/09/2024, Available online: 08/10/2024
*to whom all correspondence should be addressed: e-mail: xingchen@hfut.edu.cn
https://doi.org/10.30955/gnj.006570

Graphical abstract

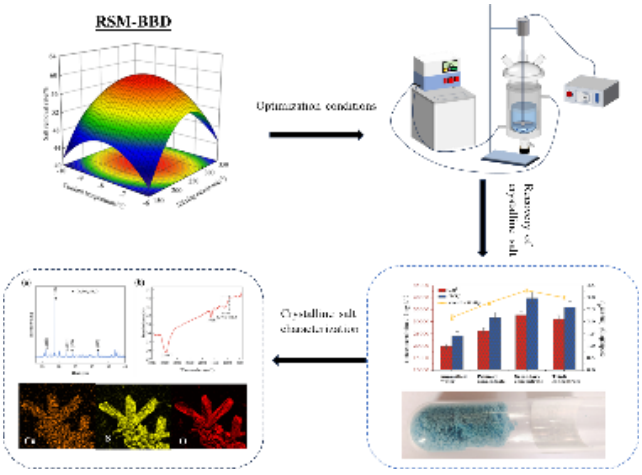

Abstract

For the copper-containing electroplating wastewater generated by a semiconductor company, the recovery of copper salts by progressive freeze crystallization and its process parameters were experimentally optimized and studied. Based on the results of single-factor experiments, according to the principles of Box-Behnken Design experimental design for response surface methodology to investigate the effects of coolant temperature, agitation rate, and freezing time on salt removal and optimize process parameters. The optimization results of the response surface method showed that the optimal conditions were when the coolant temperature was -8°C, the stirring rate was 264 r·min^{-1}, and the freezing time was 78 min. Three validation experiments were conducted under optimum conditions, and salt removal was obtained as 60.13 ± 4.10%, which is more in line with the predicted values. Treatment of copper-containing electroplating wastewater using tertiary freezing under response surface optimized experimental conditions. At this time, the total ice rate of the wastewater was about 65.00%, and the conductivity was also concentrated from 2.17 mS·cm^{-1} of the raw water to 2.99 mS·cm^{-1} with a total concentration ratio of 1.38. In addition, a higher concentration of concentrated liquid was obtained in the third freezing, while a crystalline salt precipitated from the bottom of the reactor. The precipitate was analyzed mainly as copper sulfate pentahydrate using XRD, XRF, EDS, and other characterization techniques. Theoretical calculations show that pre-cooling of raw wastewater reduces energy consumption by up to 20.40%.

Keywords: progressive freeze crystallization; response surface methodology; copper-containing electroplating wastewater; copper (II) sulfate

1. Introduction

The rapid expansion of the surface treatment industry has led to the discharge of a large amount of electroplating wastewater (Li *et al.* 2022), and acidic copper-containing electroplating sewage, as typical electroplating wastewater, is produced with strong acidity and contains a high concentration of copper ions (Li *et al.* 2021) and other characteristics. At present, electroplating wastewater treatment has entered the stage of resource reuse (Luo *et al.* 2024), and the recovery of copper salts in copper-containing electroplating wastewater can reduce environmental pollution and achieve cleaner production and resource utilization. Currently, the commonly used processes for copper-containing electroplating wastewater treatment include chemical precipitation, membrane treatment, electrodialysis technology, and evaporation and crystallization (Jeremias *et al.* 2023), of which chemical precipitation is the most widely used (Li *et al.* 2024). However, the chemical precipitation method requires adding a large number of chemicals to the water, and the secondary pollution is serious and cannot effectively recover copper salts. As an environmentally friendly wastewater treatment method, the freeze crystallization method can treat high-salt wastewater and recover crystalline salt without adding additional chemicals and less secondary pollution (Pronk *et al.* 2006). For example,

Randall *et al.* (2011) treated reverse osmosis brine using multistage freeze concentration to recover sodium and calcium sulfate.

The progressive freeze crystallization method grows ice in one direction by controlling the growth of a one-dimensional ice front (i.e., the interface between the solution and the solid phase), while concentrating impurities in the liquid phase. The main advantage of the progressive freeze crystallization method over other freezing processes is that the brine can be focused outside the ice layer, making it easy to separate the brine from the ice crystals, reducing operating costs (Samsuri *et al.* 2016). During freeze crystallization, if the rejected solute does not diffuse into the liquid phase, a highly concentrated layer forms near the moving ice-liquid interface, and the solute tends to be trapped in the ice as it grows (Luo *et al.* 2010). To avoid the solute at the interface being trapped in the ice crystals, this can be achieved by controlling the ice crystals' growth rate and the solute's mass transfer coefficient (Gu *et al.* 2010). The freezing time and coolant temperature determine the ice crystal growth rate, and the stirring rate determines the mass transfer coefficient. Therefore, in this paper, coolant temperature, freezing time, and stirring rate are chosen as independent variables to explore their effects on the purity of ice crystals. However, when more influencing factors exist, the single-factor test requires several trial times, and the interaction between the factors is difficult to grasp. The use of response surface methodology is effective in reducing the number of trials, and the two-by-two interactions between factors can be examined through response surface plots and contour plots and the resulting response surface model is also helpful in determining the optimal conditions for a multivariate system (Li *et al.* 2023).

This experiment adopted the progressive freeze-crystallization method to treat high-salt copper-containing electroplating wastewater. The effects of coolant temperature, stirring rate, and freezing time on the salt removal rate were studied deeply. The process parameters were optimized by using the response surface method, which provides a reliable basis for the feasibility study of the practical engineering application. In addition, this experiment proposes using a three-stage freezing procedure to treat copper-containing electroplating wastewater to recover the copper salts in the wastewater (van der Ham *et al.* 1999), thus achieving the resourceful use of wastewater.

2. Materials and methods

2.1. Experimental wastewater

Copper-containing electroplating wastewater was taken from a semiconductor company in Hefei, and the quality of raw water is shown in **Table 1**. From the table, it can be seen that the salt composition of copper-containing electroplating wastewater compared with the dye chemical wastewater, the composition is relatively single, mainly for copper ions and sulfate ions.

2.2. Experimental setup

Figure 1 shows the schematic diagram of the experimental setup, which mainly includes a cryostat (Shanghai Hengping DC 3010), a double-layer glass reactor, and a mechanical stirrer. Cryostats with advanced digital controllers are the main devices in progressive freeze crystallization experiments. The unit uses anhydrous ethanol as the freezing medium. When the circulating pump carries out the external circulation of coolant, the 'outlet' pipe is connected to the inlet and outlet of the experimental vessel outside the trough so that the temperature is evenly distributed and the temperature can be adjusted as low as -30°C. The temperature of the anhydrous ethanol in the cryostat can be monitored and read directly from the digital display panel on the unit. The double glass reactor was designed in-house and customized locally; the unit is a 1 L glass crystallizer with an internal diameter of 110 mm. Two ports on the side of the reactor body are connected to the cryostat tank to provide coolant and heat exchange with the solution. The coolant is fed into the glass sandwich of the reactor through the lower port and circulates upwards, leaving through the upper port. There is a downdraft valve at the bottom of the reactor. The top of the stirrer is fixed on a stand, and a digital display controller connected to the stirrer controls the stirring rate in real time.

Table 1. Copper-containing electroplating wastewater quality analysis results

Items	Content($mg \cdot L^{-1}$)
COD	2500
NH_3-N	228
TN	1309
SO_4^{2-}	24166
Cl^-	1360
PO_4^{3-}	814
Zn^{2+}	46
Cu^{2+}	19780

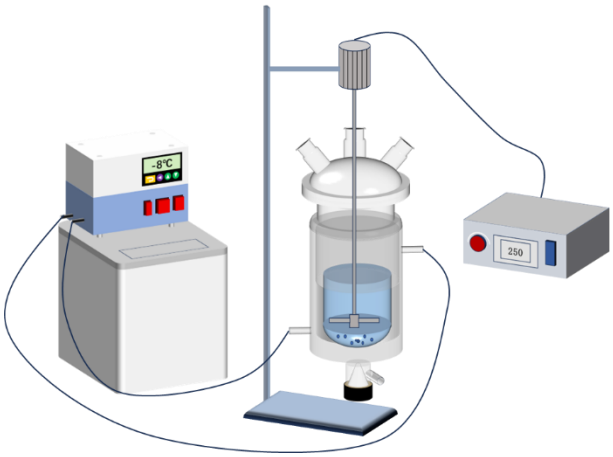

Figure 1. Schematic diagram of the experimental setup

2.3. Experimental procedure

To minimize the effect of overcooling at the initial moment of ice crystal formation, the plating wastewater was pre-cooled to near 0°C before freezing. The temperature of the freeze concentration unit was set before the start of the experiment, and to ensure that the effect of stirring rate

influence was the same for each experiment, stirring bars of the same length were submerged in the liquid. Once an ice layer is formed, stop the digital stirrer and separate the concentrate from the ice. Water quality indicators such as conductivity and ion concentration were subsequently determined for the concentrate and effluent (ice melt). In the multi-stage freezing process, the concentrate is taken and the above steps are repeated to obtain the effluent and the secondary concentrate, and the three-stage freezing process is used in this test. During the third freeze, in addition to the ice crystals generated, a blue crystalline substance precipitated from the bottom of the wastewater. The concentrate was centrifuged in a centrifuge to obtain blue crystals. The blue crystals from centrifugation were dried in a vacuum oven at 80°C. XRD, FT-IR, EDS, and XRF analyzed the precipitated crystals.

2.4. Methods of analysis

Conductivity is commonly used to measure the number of inorganic ions in water and is closely related to the concentration of soluble inorganic substances in water. A conductivity meter (DDS-307A) was used in the experiment to measure the salt concentration in the solution:

$$E = \frac{C_0 - C_s}{C_0} \times 100\% \quad (1)$$

Where E is the salt removal rate, %; C_0 is the conductivity of the initial wastewater, mS·cm^{-1}; C_S is the conductivity of the effluent, mS·cm^{-1}.

N indicates the concentration coefficient of concentration, i.e. the concentration ratio of the concentrate to the raw water, the larger the N value, the better the concentration effect:

$$N = \frac{C_L}{C_0} \quad (2)$$

Where N is the concentration ratio; C_0 is the conductivity in the initial wastewater, mS·cm^{-1}; C_L is the conductivity in the concentrate, mS·cm^{-1}.

The ice formation rate is the volume of water recovered as ice at the end of the experiment relative to the volume of the feed:

$$I = \frac{M_0 - M_S}{M_0} \times 100\% \quad (3)$$

Where I is the ice formation rate, %; M_0 is the volume of the initial wastewater, L; M_S is the volume of the effluent, L.

Anions are analyzed by ion chromatography for concentration analysis, and cations are analyzed by an Inductively Coupled Plasma (ICP) analyzer. Before testing, the solution needs to be permeabilized. For copper-containing electroplating wastewater, three-stage freezing and concentration to get out of the water and concentrate, because in the freezing process did not occur chemical changes, so theoretically out of the water and concentrate should be with the original water between the material calculations should meet the formula (4), in line with the law of conservation of mass.

$$A_0 \times M_0 = A_S \times M_S + A_L \times M_L \quad (4)$$

Where A_0 is the ion content in the initial wastewater, mg·L^{-1}; A_S is the ion content in the effluent, mg·L^{-1}; A_L is the ion content in the concentrate, mg·L^{-1}.

2.5. Characterization of precipitates

Scanning Electron Microscope (SEM), a high-resolution emission scanning electron microscope (Regulus 8230, Hitachi, Japan), was used to microscopically image the surface of the precipitated solid. An appropriate amount of the precipitated solid was placed in anhydrous ethanol, and a homogeneous dispersion was prepared using ultrasound. Subsequently, a small amount of the dispersion was taken and dropped onto a smooth monocrystalline silicon wafer substrate, which was allowed to dry naturally. Energy Dispersive Spectrometer (EDS), a Bruker X-Flash 60 energy spectrometer, was used to perform the EDS analysis to determine the elemental content of the precipitates.

Fourier Transform Infrared Spectroscopy (FT-IR), an FT-IR spectrometer (Nicolet IS50 iN10, Thermo Nicolet, USA), was used to do functional group analysis of the precipitated substances.

X-ray powder Diffraction (XRD) was used to analyze the crystal structure of the samples using an X-ray diffractometer (Rigaku D/MAX2500VL/PC, Rigaku Corporation, Japan) under the following test conditions: the Cu target Kα was used as the source of diffraction, and the diffracted rays were diffracted at a wavelength of λ=1.54Å, and the scanning range2θ was5°~90°.

X-Ray Fluorescence (XRF): A certain amount of dry sample is taken and placed on a carrier sheet specially designed for X-Ray Fluorescence testing, compacted, and placed on a sample stage for testing. With the help of an X-ray fluorescence spectrometer, the sample is analyzed for its elemental species and content.

3. Results and discussion

3.1. Effect of coolant temperature on salt removal rate

(1) The effect of coolant temperature on salt removal is shown in **Figure 2**. The effect of temperature from -4 to -12°C on the salt removal rate was investigated at an agitation rate of 250 r·min^{-1} and a freezing time of 90 min. As the temperature increases, the salt removal first increases and then decreases to increase, the temperature reaches -8℃, and the removal rate reaches the highest value. This is because temperature is the main factor affecting the ice crystal growth rate (Miyawaki *et al.* 2005), which increases with the difference between the solution and coolant temperatures (Flesland, 1995). The decrease in coolant temperature increases the ice crystal growth rate, which exceeds the solute diffusion rate (Chen *et al.* 1998) , and promotes solute entrapment in the ice crystals. Thus, low growth rates produce high-purity ice. In contrast, at -4°C and -6°C, unsmooth and very thin dendritic ice crystals are formed due to heterogeneous nucleation (Wang *et al.* 2019), and the resulting ice crystals have a higher rate of solute entrapment, which leads to lower purity of ice crystals (Mountadar *et al.* 2019).

(2)The effect of stirring rate on salt removal is shown in **Figure 3**. **Figure. 3** shows the effect of coolant temperature and freezing time fixed at -8°C and 90 min, respectively, where the stirring rate was 50 to 450 r·min^{-1}on the salt removal rate. From the figure, it can be seen that the salt removal is maximum at a stirring rate of 250 r·min^{-1}. Stirring rate is also an important parameter in progressive freeze crystallization as it plays an important role in reducing the solute concentration in the vicinity of ice crystals. Dendritic ice structures formed by structural supercooling can also be avoided by providing a suitable stirring rate, leaving firmer and higher-quality ice crystals (Shirai *et al.* 1998). However, if the stirring rate is too high, the ice crystals generated will mix with the solute, making the ice layer less pure.

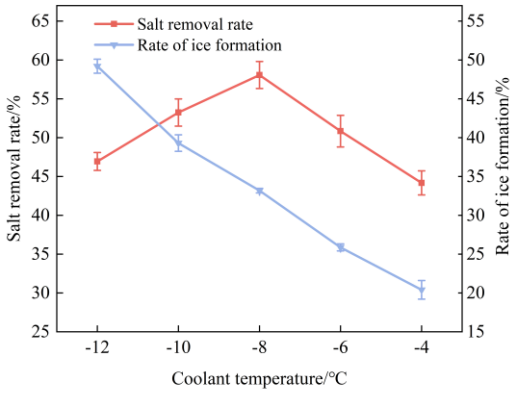

Figure 2. Effect of coolant temperature on salt removal rate

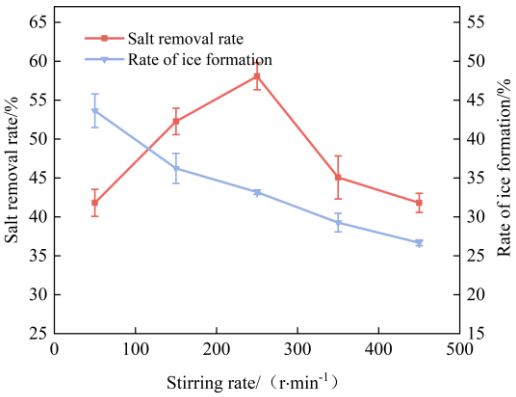

Figure 3. Effect of stirring rate on salt removal rate

(3)The effect of freezing time on salt removal is shown in **Figure 4**. At a temperature of -8°C and an agitation rate of 250 r·min^{-1}, the removal rate increased substantially with increasing freezing time, reaching a maximum value at 90 min of freezing time. This is because the ice crystal growth rate is high at the start of freezing. Still, over time, the thickness of the ice layer increases, and the efficiency of heat transfer between the coolant and the solution decreases, resulting in a lower ice crystal growth rate. In addition, higher accumulation of solutes at the solid-liquid interface will lower the freezing point of the solution, thus making it more difficult for freeze crystallization to occur (Chen *et al.* 1998). However, after 90 min of freezing, the trend changes. When the cooling time is too long, due to the small area in the container, the remaining liquid is saturated with solutes, and a large amount of solute in the solution can easily be trapped in the ice if the freezing process continues.

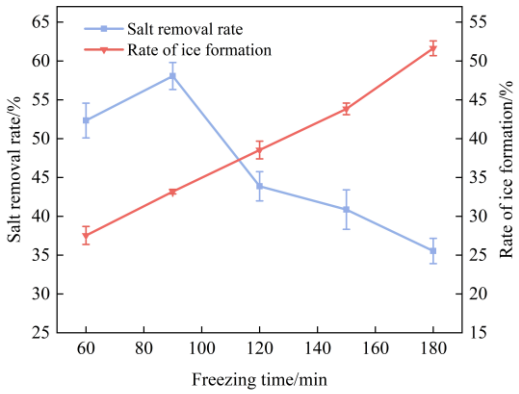

Figure 4. Effect of freezing time on salt removal rate

3.2. Response surface methodology optimization

3.2.1. Model building and analysis of variance

Response surface methodology was used for the process optimization of salt concentration in the progressive freeze crystallization method, and the optimized level of each factor determined by a one-way experiment was used as the central level of the BBD experimental design. Coolant temperature, stirring rate, and freezing time were used as independent variables, and salt removal rate was the response value. Two-by-two interactions between the three factors were examined to determine optimal freezing conditions and response values. Based on the BBD experimental principle, a three-factor, three-level experimental design table was designed as shown in **Table 2**. With +1 for the high level, -1 for the low level, and 0 for the center level (Fu *et al.* 2020). The experimental set of Box-Behnken designs is shown in **Table 3**, where 17 experiments were performed to obtain a quadratic model consisting of 12 experiments plus 5 replicated centroids. To avoid systematic errors, the experiments were randomized. **Table 3** shows the design and results of progressive freeze crystallization experiments based on the BBD experimental design, with observed values of salt removal ranging from 41.29% to 60.81%.

Table 2. Response surface factors and levels based on BBD experiments

Symbols	Levels		
	-1	**0**	**+1**
Temperature/°C	-10	-8	-6
Stirring rate /(r·min^{-1})	150	250	350
Time /min	60	90	120

Experimental results were created, evaluated, and optimized using Design Expert 11 software. The following fitted second-order polynomial equation represents the empirical relationship between the response and the variables (Pandey *et al.* 2018):

$$E(\%) = 59.8 + 0.4A + 1.08B - 2.3C + 0.4AB - 0.1AC - 3.2BC - 6.6A^2 - 10.6B^2 - 4.5C^2 \quad (5)$$

where E is the salt removal rate, and A, B, and C represent the coolant temperature, stirring rate, and freezing time, respectively. From equation (5), it can be seen that freezing time is the most prominent influence on the response value. From a linear point of view, A, B, and AB have positive coefficients indicating synergistic effects, while the quadratic terms A^2, B^2, C^2, and C, AC, and BC have negative coefficients indicating antagonistic effects on salt removal rates (Bajpai *et al.* 2021).

Before analyzing the model's response surface and contour plots, it is usually necessary to perform an ANOVA on the experimental results and check the significance of the fitted model. The results of the ANOVA are shown in **Table 4**, where A is the coolant temperature, B is the stirring rate, and C is the freezing time. The model's accuracy was measured using the correlation coefficient R^2, the closer R^2 is to 1, the more accurate the model is (Alrugaibah *et al.* 2021). The model correlation coefficient R^2 is 98.97%, higher than 95%, indicating that the model explains the experimental results well. In addition, the R^2_{Adj} of the model is 97.64%, and the R^2_{Pred} is 89.23%, and the difference between the values of R^2_{Adj} and R^2_{Pred} is within 0.2, which indicates that the model results are reasonable (Inger *et al.* 2019). If Adequate precision is much higher than 4, the simulation results have a high degree of confidence and are subject to little interference (Ji *et al.* 2023).

Table 3. BBD experimental design and results

Run	Independent variable			Response value
	Temperature(℃)	Stirring rate(r·min^{-1})	Times(min)	Salt removal rate(%)
1	-8	250	90	59.05
2	-6	250	60	50.81
3	-6	150	90	42.7
4	-10	150	90	41.29
5	-8	250	90	59.69
6	-8	150	60	42.2
7	-10	250	120	46.7
8	-8	250	90	58.69
9	-10	350	90	41.7
10	-8	350	120	40.67
11	-10	250	60	51.3
12	-8	350	60	51.74
13	-6	250	120	45.9
14	-8	150	120	44.1
15	-8	250	90	60.72
16	-6	350	90	44.8
17	-8	250	90	60.81

Table 4. Analysis of variances

np	Sum of squares	Degrees of freedom	Mean square	F-value	P-value	
Model	911.44	9	101.27	74.52	< 0.0001	Significant
A	1.30	1	1.30	0.95	0.3613	
B	9.29	1	9.29	6.83	0.0347	
C	43.62	1	43.62	32.10	0.0008	
Residual	9.51	7	1.36			
Lack of fit	5.84	3	1.95	2.12	0.2404	Not Significant

R^2 = 0.9897

Adjust R^2 = 0.9764

Predicted R^2 = 0.8923

Adequate precision = 21.94

3.2.2. Response surface analysis

From **Figure 5(a)-Figure 5(c)**, it can be seen that the salt removal rate increased and then decreased as the coolant temperature increased from -10°C to -6°C, the stirring speed increased from 150 r·min^{-1} to 350 r·min^{-1}, and the freezing time increased from 60 min to 120 min, which indicates that either too high or low coolant temperature, stirring speed and freezing time all lead to the decrease of salt removal rate.

The contour plot of **Figure 5(d)** is obtained by projecting the response surface plot of **Figure 5(a)** on the bottom surface, and from the contour plot, it can be seen that the density of contours in the direction of the stirring rate is higher than that in the direction of coolant temperature. It can be deduced that the stirring rate affects the salt removal rate to a greater extent than the coolant temperature. The contour plot of **Figure 5(e)** is obtained by projecting the response surface plot of **Figure 5(b)** on the bottom surface, and from the contour plot, it can be seen

that the concentration of contour lines in the direction of freezing time is higher than that in the direction of coolant temperature, and it can be deduced that the freezing time affects the salt removal rate to a greater extent than the coolant temperature. The contour plot of **Figure 5(f)** was obtained from the projection of the response surface of **Figure 5(c)** on the bottom surface, from which it can be seen that the salt removal rate showed an increasing and then decreasing trend with the increase of freezing time and agitation rate. In addition, its contour shape was closest to an ellipse, proving the most significant interaction between freezing time and stirring rate(Priya and Kanmani, 2011). In addition, the density of contours in the direction of freezing time is higher than that in the direction of the stirring rate, and it can be inferred that the freezing time affects the salt removal rate to a greater extent than the stirring rate.

According to the above analysis, the magnitude of the effect of coolant temperature, stirring rate, and freezing time on the salt removal rate was in the order of freezing time > stirring rate > coolant temperature, which is consistent with the results of the ANOVA model.

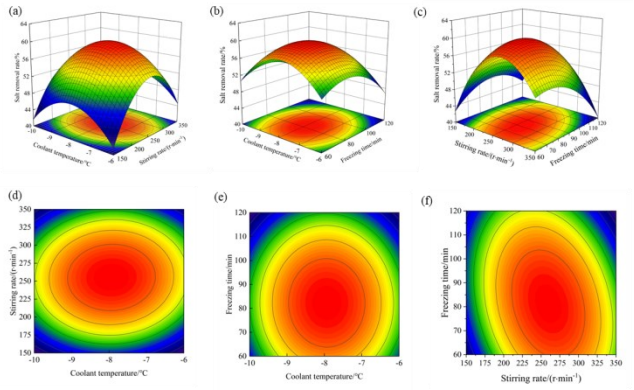

Figure 5. Response surface plots of the effect of (a) coolant temperature and agitation rate, (b) coolant temperature and freezing time, (c) agitation rate and freezing time on salt removal, and contour plots of the effect of (d) coolant temperature and agitation rate, (e) coolant temperature and freezing time, (f) agitation rate and freezing time on salt removal

3.2.3. Optimization and validation of results

In the optimization process, the Derringer function can be used, which can optimize the response values. The targets for coolant temperature, stirring rate, and freezing time were set to "in range", and the target for salt removal rate was set to "maximum". The optimal conditions for optimizing the salt removal rate can be obtained from the above settings: -8°C, 78 min, 264 r·min^{-1}, and the predicted salt removal rate under these conditions is 60.13%. Three experimental validations of the optimal conditions obtained gave a salt removal rate of 60.13 ± 4.1%, which is more in line with the theoretical values.

3.3. Tertiary freezing treatment of copper-containing electroplating wastewater

The change in conductivity of the concentrate after the three-stage freezing process is shown in **Figure 6**. At a total ice formation rate of about 65.00 %, the concentration ratio for the conductivity of the primary concentrate is 1.28, the concentration ratio for the conductivity of the secondary concentrate is 1.18, and the total concentration ratio is 1.38. Compared with the experimental data of primary freezing, the conductivity concentration ratio of secondary freezing is low, which may be analyzed because of the higher concentration of the secondary concentrate compared with the primary concentrate, and when the concentration of the solution increases, its freezing point decreases, the degree of subcooling and the ice growth rate increase, and the stability of the solid-liquid interface decreases, and the dendritic ice crystals come into being. In addition to this, the interactions between the molecules lead to higher solution viscosity and lower solute diffusion rate when the solution concentration increases. That is, the higher the solution concentration, the more potential nuclei in solution, the increasing frequency of nuclei colliding with each other and the energy consumed, thus enhancing secondary nucleation as well as the formation of small crystal sizes (dendrites) (Amran *et al.* 2016), and ice crystals of this structure lead to the trapping of more impurities or solutes into the ice.

As shown in **Figure 6**, the changes in the concentration of copper and sulfate ions in the concentrate followed the same trend as that of the conductivity, with the concentration of copper and sulfate ions in the concentrate increasing step by step in both the first and second freezing phases, whereas the third concentrate showed a slight decrease in comparison with the second concentrate instead. This change may be because after the solution reaches its concentration limit during the third freezing process, the concentration no longer increases, and solutes are precipitated. A total of 2.0 g of solids were precipitated in the effluent from the third freezing process.

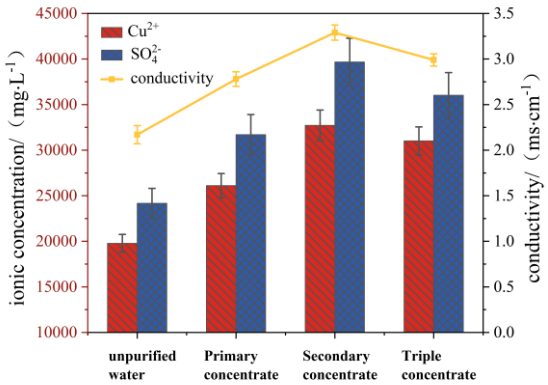

Figure 6. Changes in conductivity and ion concentration of concentrate during tertiary freezing

3.4. Analysis of precipitates

Approximately 2.0 g of blue crystals were obtained after centrifugation and vacuum drying of the solids precipitated during progressive freeze crystallization of copper-containing electroplating wastewater as shown in **Figure 7**. The solids were analyzed by XRD, FT-IR, EDS, and XRF to determine their main components.

Figure 8(a) shows the XRD patterns of the precipitates. Compared with the standard XRD card of copper sulfate pentahydrate (JCPDS No. 11-0646), it can be seen that the diffraction peaks of the precipitated crystals appeared at

2θ=16.16°, 19.03°, 22.21°, 23.97°, and 31.66°, which corresponded to (1♠0), (110), (011), (♠21), (1↔1) crystal planes, which are all characteristic diffraction peaks of copper sulfate pentahydrate.

Figure 7. Solids from the tertiary freezing treatment of copper-containing electroplating wastewater

Figure 8(b) shows the FT-IR spectrum of the precipitated crystals, according to the spectral library, for the similarity comparison analysis from the figure. It can be seen that there is a distinct peak at 3343.7 cm^{-1} wavelength for the stretching vibration of the conjugated hydroxyl group (-OH); 1517.2 cm^{-1}~1750.1 cm^{-1} there is a sharp peak of absorption, the peak position is 1628.1 cm^{-1}, and this peak was determined to be the water of crystallization variable angle vibration peak (Nagabhushana *et al.* 2009). A broader spectral peak appeared in the wavelength range of 915.5 cm^{-1}~1246.3 cm^{-1}, which was judged to be the telescopic vibrational absorption peak of sulfate (SO_4^{2-}) (Teixeira dos Santos *et al.* 2016), so it was presumed that there was sulfate in the precipitated solid, which was in agreement with the previous presumed results.

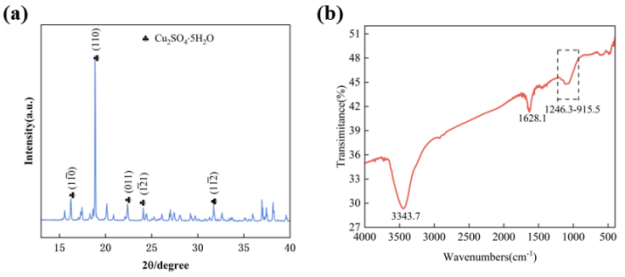

Figure 8. (a) XRD patterns, (b) FT-IR spectrum

The surface micromorphology of the precipitates is shown in the SEM image of **Figure 9**. From the solid surface micromorphology in the figure, we can see that the crystals of the precipitates obtained in the crystallization process show a columnar morphology. To further confirm the elemental composition of the precipitates, the EDS spectra of the precipitates were analyzed, as shown in **Figure 9**, and the main elements detected in the solids were Cu, O, and S.

The mass percentages and atomic number percentages of the major elements in the precipitates are shown in **Table 5**, with approximately 34.94 %, 53.53 %, 11.53%, and 12.92 %, 78.62 %, and 8.45 % for the elements Cu, O, and S, respectively. Analyzed in conjunction with the previous FT-IR and XRD results, the precipitate contains a certain amount of copper sulfate pentahydrate.

XRF analyzed the material composition of the precipitates, and according to the XRF results, the main elements in the precipitates were Cur and S with 56.97% and 16.34%, respectively, and contained a small amount of Cl with 2.34%. Combined with the analysis of FT-IR, XRD, and EDS spectra of the precipitates, it can be seen that the main component of the precipitates is copper sulfate pentahydrate.

Table 5. The mass percentage and atomic number percentage of each element in the precipitates

Element	Mass norm(%)	Atom(%)
S	11.53	8.45
O	53.53	78.62
Cu	34.94	12.92
	100.00	100.00

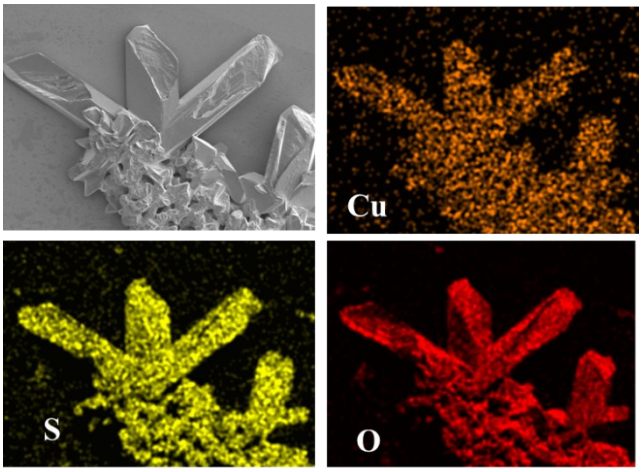

Figure 9. Element mapping of precipitates

3.5. Material balance

During the tertiary freezing process, we analyzed the water quality of the ice meltwater and concentrate obtained from each freezing stage. **Table 6** shows the variation of ionic concentration in the inlet and outlet water of copper-containing electroplating wastewater under the response surface optimization experimental conditions. Theoretically, there is a material balance between the inlet and outlet water. Still, considering the loss of material caused by washing ice crystals in the freezing process, experimental errors, and other issues, there is an error between the two. (Chen *et al.* 2019). As seen in **Table 6**, compared with the feed water, the copper ion content and sulfate content in the secondary concentrate increased to 65.44% and 64.18% of the feed water, respectively. Therefore, $CuSO_4$ can be isolated and recovered by treating the secondary concentrate with progressive freeze co-crystallization. Calculation of the copper ion and sulfate content of the concentrate and effluent obtained from the third stage of freezing revealed a reduction of 1.01 g and 1.38 g, respectively, as compared to the second stage concentrate, whereas 2.00 g of crystalline salt was recovered in this experiment.

3.6. Energy consumption analysis

This experiment is a three-stage freeze crystallization, and its theoretical energy consumption is divided into three main parts: one part is used for the energy required to cool down the wastewater to the crystallization temperature; one part is used for the energy consumed by the water to undergo a phase change, and one part is used for the energy consumed by the ice to continue to cool down to the freezing temperature. Assuming an effluent yield of

500 kg·h^{-1}, an initial wastewater temperature of 20°C, a freezing temperature of -8°C, and an ice formation rate of 50%.

$$Q = C_W M\Delta t_1 + M\Delta_{fus}H \times 0.5 + C_I M\Delta t_2 \times 0.5 \quad (6)$$

where C_W is the specific heat capacity of wastewater, taken as 4.2 kJ^{-1}·kg^{-1}·°C^{-1}; M is the mass of wastewater; Δt_1 is the temperature difference of wastewater cooling; $\Delta_{fus}H$ is the enthalpy of melting of ice, taken as 333.5 kJ·kg^{-1}; C_I is the specific heat capacity of ice, taken as 2.06 kJ^{-1}·kg^{-1}·°C^{-1}; Δt_2 is the temperature difference of ice cooling.

Therefore, the electrical power required for this cryogenic process is:

$$E = \frac{Q}{COP \times T} \quad (7)$$

Where COP is the cooling coefficient of the refrigeration unit; T is the time (s).

In the freeze crystallization process, when the refrigeration unit is operated in an ideal inverse Carnot cycle, the refrigeration performance factor is:

$$COP = \frac{TL}{TH - TL} \quad (8)$$

Where TL is coolant temperature, K; TH is room temperature, K.

Table 6. Test results of dye chemical wastewater before and after treatment

Detection indicators	Water	Single freezing		Secondary freezing		Tertiary freezing	
		Effluent	Concentrate	Effluent	Concentrate	Effluent	Concentrate
Cu^{2+}(mg·L^{-1})	19780	7463	26110	10442	32724	13744	31019
SO_4^{2-}(mg·L^{-1})	24166	9502	31705	12714	39675	16504	36020
Volumetric(mL)	300	95	200	60	135	40	92

In the primary freezing process Δt_1 is 24°C, Δt_2 is 4°C, M is 250 kg, and the electrical power required for the freezing process, E_1 = 3.97 kW, is calculated from Eq. 6 and Eq. 7. For the secondary freezing process, the wastewater temperature is 0°C, so Δt_1 is 4°C and M is around 250 kg, so E_2 = 1.37 kW. During the tertiary freezing process, a part of the energy consumption is used for the crystallization of solids, which is negligible in view of the fact that it is small compared to the energy consumption of the frozen wastewater. Therefore, the electrical power for tertiary freezing was obtained as E_3 = 0.69 kW. At this point, the total power E = 6.03 kW.

After freeze-crystallization treatment, the wastewater is divided into a low-temperature concentrate and an ice layer, and to make full use of this cold energy, the concentrate and the ice layer can be used to pre-cool the original solution to reduce the temperature of the original solution, thus reducing the energy consumption of the freeze-crystallization process. Pre-cooling the wastewater before treatment using ice and concentrate from the freeze crystallization process allows the wastewater to be pre-cooled to a lower temperature before freezing, taking t = 0°C. At this point, Δt_1=4°C and E_1=2.74 kW. From the above results, it can be seen that there is a reduction in freezing energy consumption after pre-cooling, with up to 20.40% reduction in energy consumption after pre-cooling as compared to non-pre-cooling energy consumption. The above energy consumption analyses are theoretical calculations, and the actual energy consumption needs to be verified in engineering practice.

4. Conclusion

(1) A response surface methodology for BBD experimental design was used to develop a regression model to predict salt removal efficiency. The results of response surface and contour plot analyses showed that the degree of influence of the three factors on the salt removal rate was in the order of freezing time > stirring rate > coolant temperature. The optimum conditions were derived as -8°C, freezing time 78 min, stirring rate 264 r·min$^{-1,}$ and the predicted value of salt removal under these conditions was 60.13%. Three validation experiments were conducted on this. The results showed that the salt removal rate was 60.13 ± 4.1%, similar to the simulated predictions, indicating that this model can accurately simulate the experimental results.

(2) The tertiary freezing method treated copper-containing electroplating wastewater under optimized freezing conditions by response surface methodology. The results showed that the total ice formation rate during the tertiary freezing process was about 65.00 percent, and the conductivity concentration ratio was 1.38. Crystalline salt precipitated during tertiary freezing, and the main component of the precipitated solid material was judged to be copper sulfate pentahydrate by XRD, FT-IR, EDS, and XRF characterization and analysis.

References

Alrugaibah M., Yagiz Y. and Gu L.W. (2021), Use natural deep eutectic solvents as efficient green reagents to extract procyanidins and anthocyanins from cranberry pomace and predictive modeling by RSM and artificial neural networking. *Separation and Purification Technology*, 117720.

Amran A.N., Safiei Z.N., Samsuri S., Zakaria, Y.Z., Jusoh and Mazura. (2016). Review: Parametric Study on the Performance of Progressive Cryoconcentration System. *Chemical Engineering Communications*, **203**(7), 957–975.

Bajpai M., Katoch S.S., Kadier A. and Ma P.C. (2021), Treatment of pharmaceutical wastewater containing cefazolin by electrocoagulation (EC): Optimization of various parameters using response surface methodology (RSM), kinetics and isotherms study. *Chemical Engineering Research & Design*, **176**, 254–266.

Chen P., Chen X.D. and Free K.W. (1998), Solute inclusion in ice formed from sucrose solutions on a sub-cooled surface—an experimental study. *Journal of Food Engineering*, **38**, 1–13.

Chen P., Wang L., Song P., Chen X., Yin Y., Liu Y., Cai L. and Zhang L. (2019). Recovering olaquindox and decreasing COD and salt concentrations in antibiotic wastewater by multiple freeze-thaw processes and crystallization. *Journal of Cleaner Production*, **225**, 248–255.

Flesland O. (1995). Freeze concentration by layer crystallization. *Drying Technology*, **13**, 1713–1739.

Fu G., Jiang J.C. and Ni L. (2020). Research-scale three-phase jet foam generator design and foaming condition optimization based on Box-Behnken design. *Process Safety and Environmental Protection*, **134**, 217–225.

Gu X., Suzuki T. and Miyawaki O. (2010). Limiting Partition Coefficient in Progressive Freeze-concentration. *Journal of Food Science*, **70**, E546–E551.

Inger M., Dobrzyńska-inger A., Rajewski J. and Wilk M. (2019). Optimization of Ammonia Oxidation Using Response Surface Methodology. *Catalysts*, **9**(3), 030249.

Jeremias J.S. D., Lin J.Y., Dalida M.L.P. and Lu M.C. (2023). Abatement technologies for copper containing industrial wastewater effluents – A review. *Journal of Environmental Chemical Engineering*, 109336.

Ji X., Wang Z. J., Zhang H.B., Wan X. F., Huo J.Y. and Zhang T.H. (2023). Optimization design and characterization of slag cementitious composites containing carbide slag and desulfurized gypsum based on response surface methodology. *Journal of Building Engineering*, 107441.

Li G., Liang Z., Sun J., Qiu Y. and Jiang F. (2021). A pilot-scale sulfur-based sulfidogenic system for the treatment of Cu-laden electroplating wastewater using real domestic sewage as electron donor. *Water Research*, 116999.

Li H.F., Ma X. and Zhang G.Z. (2023). Optimization of mortar self-healing performance-based on response surface methodology: A multifactor analysis of zeolites, crystalline admixtures, and water-to-binder ratio. *Construction And Building Materials*, 134015.

Li Q., Wang Y., Chang Z., El Kolaly W., Fan F. and Li M. (2024). Progress in the treatment of copper(II)-containing wastewater and wastewater treatment systems based on combined technologies: A review. *Journal of Water Process Engineering*, 104746.

Li S., Dai M., Wu Y., Fu H., Hou X., Peng C. and Luo H. (2022). Resource utilization of electroplating wastewater: obstacles and solutions. *Environmental Science-Water Research & Technology*, **8**, 484–509.

Luo C.S., Chen W.W. and Han W.F. (2010). Experimental study on factors affecting the quality of ice crystal during the freezing concentration for the brackish water. *Desalination*, **260**, 231–238.

Luo H., Wang J., Wang C., Luo Z. and Qu L. (2024). Decomplexation of Cu(II)-EDTA by heat assisted CuO catalyzed H_2O_2: Sequential addition of H_2O_2, kinetics, mechanism and catalyst reutilization. *Journal of Environmental Chemical Engineering*, 112800.

Miyawaki O., Liu L., Shirai Y., Sakashita S. and Kagitani K. (2005). Tubular ice system for scale-up of progressive freeze-concentration. *Journal of Food Engineering*, **69**, 107–113.

Mountadar S., Guessous M., Rich A., Karmil F.Z., Belghit H.E., Siniti M. and Tahiri S. (2019). Desalination of spent ion-exchange resin regeneration solutions by suspension freeze crystallization. *Desalination*, 114059.

Nagabhushana H., Nagabhushana B.M., Premkumar H.B., Lakshminarasappa B.N., Singh F. and Chakradhar R.P.S. (2009). Raman and infrared study of 100 MeV swift heavy ion irradiation effects in Ca_2SO_4 single crystals. *Journal of Alloys and Compounds*, **482**, 308–312.

Pandey A., Belwal T., Sekar K.C., Bhatt I.D. and Rawal R.S. (2018). Optimization of ultrasonic-assisted extraction (UAE) of phenolics and antioxidant compounds from rhizomes of using response surface methodology (RSM). *Industrial Crops and Products*, **119**, 218–225.

Priya R. and Kanmani S. (2011). Optimization of photocatalytic production of hydrogen from hydrogen sulfide in alkaline solution using response surface methodology. *Desalination*. **276**, 222–227.

Pronk P., Ferreira C.A.I. and Witkamp G.J. (2006). Influence of solute type and concentration on ice scaling in fluidized bed ice crystallizers. *Chemical Engineering Science*, **61**, 4354–4362.

Randall D.G., Nathoo J. and Lewis A.E. (2011). A case study for treating a reverse osmosis brine using Eutectic Freeze Crystallization - Approaching a zero waste process - ScienceDirect. *Desalination*, **266**, 256–262.

Samsuri S., Amran N.A., Yahya N. and Jusoh M. (2016). Review on Progressive Freeze Concentration Designs. *Chemical Engineering Communications*, **203**, 345–363.

Shirai Y., Wakisaka M., Miyawaki O. and Sakashita S. (1998). Conditions of producing an ice layer with high purity for freeze wastewater treatment. *Journal of Food Engineering*, **38**, 297–308.

Teixeira DOS Santos C.A., Páscoa R.N.M.J., Porto P.A.L.S., Cerdeira A.L. and Lopes J.A. (2016). Application of Fourier-transform infrared spectroscopy for the determination of chloride and sulfate in wines. *LWT - Food Science and Technology*, **67**, 181–186.

Vanderham F., Witkamp G.J., De Graauw J. and Van Rosmalen G.M. (1999). Eutectic freeze crystallization simultaneous formation and separation of two solid phases. *Journal of Crystal Growth*, **198–199**, 744–748.

Wang T.B., Lü Y.J., Ai L.Q., Zhou Y.S. and Chen M. (2019). Dendritic Growth Model Involving Interface Kinetics for Supercooled Water. *Langmuir*, **35**, 5162–5167.